Solution Structure and Activity of the Synthetic Four-Disulfide Bond Mediterranean Mussel Defensin (MGD-1)

Yin-Shan Yang,[‡] Guillaume Mitta,[§] Alain Chavanieu,[‡] Bernard Calas,[‡] Jean Frédéric Sanchez,[‡] Philippe Roch,[§] and André Aumelas*,[‡]

Centre de Biochimie Structurale, CNRS UMR 5048, INSERM U414, Université Montpellier 1, Faculté de Pharmacie, 15 avenue Charles Flahault, 34060 Montpellier Cedex 2, France, and Défense et Résistance chez les Invertébrés Marins (DRIM), UMR 5098, Université Montpellier 2, CC80 Place Eugène Bataillon, 34095 Montpellier Cedex 5, France

Received May 24, 2000; Revised Manuscript Received August 21, 2000

ABSTRACT: MGD-1 is a 39-residue defensin-like peptide isolated from the edible Mediterranean mussel, *Mytilus galloprovincialis*. This peptide is characterized by the presence of four disulfide bonds. We report here its solid-phase synthesis and an easy way to improve the yield of the four native disulfide bonds. Synthetic and native MGD-1 display similar antibacterial activity, suggesting that the hydroxylation of Trp28 observed in native MGD-1 is not involved in the antimicrobial effect. The three-dimensional solution structure of MGD-1 has been established using ^{1}H NMR and mainly consists of a helical part (Asn7−Ser16) and two antiparallel β-strands (Arg20−Cys25 and Cys33−Arg37), together giving rise to the common cystine-stabilized $\alpha-\beta$ motif frequently observed in scorpion toxins. In MGD-1, the cystine-stabilized $\alpha-\beta$ motif is stabilized by four disulfide bonds (Cys4−Cys25, Cys10−Cys33, Cys14−Cys35, and Cys21−Cys38), instead of by the three disulfide bonds commonly found in arthropod defensins. Except for the Cys21−Cys38 disulfide bond which is solvent-exposed, the three others belong to the particularly hydrophobic core of the highly constrained structure. Moreover, the C4−P5 amide bond in the cis conformation characterizes the MGD-1 structure. MGD-1 and insect defensin A possess similar bactericidal anti-Gram-positive activity, suggesting that the fourth disulfide bond of MGD-1 is not essential for the biological activity. In agreement with the general features of antibacterial peptides, the MGD-1 and defensin A structures display a typical distribution of positively charged and hydrophobic side chains. The positively charged residues of MGD-1 are located in three clusters. For these two defensin peptides isolated from insects and mollusks, it appears that the rather well conserved location of certain positively charged residues and of the large hydrophobic cluster are enough to generate the bactericidal potency and the Gram-positive specificity.

Antimicrobial peptides are usually cationic and classified into three families: cysteine-rich, α-helical, and proline- or glycine-rich peptides (*1*, *2*). Defensins are antimicrobial peptides isolated from mammals, arthropods, and plants; they belong to the cysteine-rich family. Mammalian defensins comprise the human neutrophil peptides (HNP-1−4),[1] human defensins (HD-5 and -6), two human β defensins (HBD-1 and -2) (*3*, *4*), and recently a cyclic rhesus theta defensin (RTD-1) (*5*). A great number of defensins have also been isolated from arthropods (*6*) and plants (*7*). Although all defensins display antibacterial activity, mammalian and other vertebrate defensins are quite different from the arthropod defensins in terms of both sequence and structure (*8*−*10*).

Four peptides displaying an interesting sequence homology with several arthropod defensins were isolated from marine bivalve mollusks. All these peptides share the insect defensin signature including six cysteines. Two defensin-like peptides of 37 and 35 residues, termed peptide A and peptide B, respectively, were isolated from mussels (*Mytilus edulis*) harvested in the White Sea (*11*). At the same time, another defensin of 38 residues was isolated from the edible Mediterranean mussel (*Mytilus galloprovincialis*) (*12*), and later, a second isoform from its cDNA was identified (*13*). These two defensins termed MGD-1 and MGD-2 (MGD for *M. galloprovincialis* defensin) were found to contain eight cysteine residues involved in four disulfide bridges instead of three as for peptides A and B. A further sequence analysis

* To whom correspondence should be addressed: Centre de Biochimie Structurale, CNRS UMR 5048, INSERM U414, Faculté de Pharmacie, 15 avenue Charles Flahault, F-34060 Montpellier Cedex 2, France. Telephone: 33 (0)4 67 04 34 32. Fax: 33 (0)4 67 52 96 23. E-mail: aumelas@cbs.univ-montp1.fr.

‡ Université Montpellier 1.

§ Université Montpellier 2.

[1] Abbreviations: CD, circular dichroism; CS$\alpha\beta$ motif, cystine-stabilized $\alpha-\beta$ motif; CSH motif, cystine-stabilized α-helical motif; 1D and 2D, one- and two-dimensional, respectively; DG, distance geometry; DQF-COSY, 2D double-quantum-filtered correlation spectroscopy; GSH and GSSG, reduced glutathione and oxidized glutathione, respectively; HBD, human β defensins; HNP, human neutrophil peptide; MALDI-TOF, matrix-assisted laser desorption/ionization-time-of-flight; MBC, minimal bactericidal concentration; MD, molecular dynamics; MIC, minimal inhibitory concentration; MGD-1, *M. galloprovincialis* defensin; NMR, nuclear magnetic resonance; NOE, nuclear Overhauser effect; NOESY, 2D nuclear Overhauser effect spectroscopy; rmsd, root-mean-square deviation; RP-HPLC, reverse-phase high-performance liquid chromatography; RTD, rhesus θ defensin; SA, simulated annealing; TOCSY, total correlation spectroscopy; TPPI, time-proportional phase incrementation; TSP-d_4, sodium 2,2,3,3-tetradeuterio-3-(trimethylsilyl)propionate.

10.1021/bi0011835 CCC: $19.00
Published on Web 11/01/2000

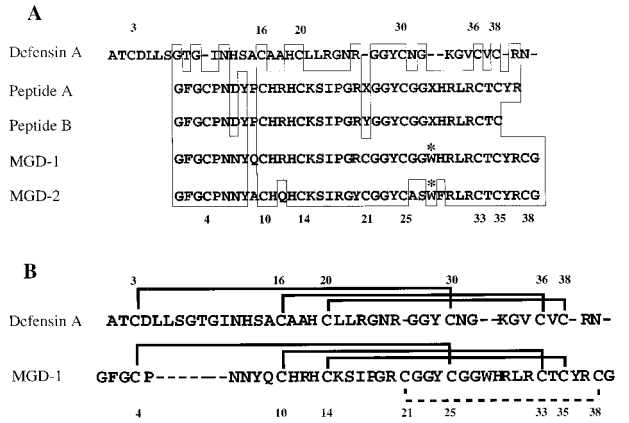

FIGURE 1: (A) Sequence alignments of defensin A, whose three-dimensional structure is known (PDB entry 1ica), with peptides A and B isolated from *M. edulis* and with MGD-1 and MGD-2 peptides isolated from *M. galloprovincialis*. The four mussel peptides display a very high level of sequence identity. MGD-1 and defensin A display a level of sequence identity of 38.5%. For all these peptides, the positions of five cysteine residues out of eight are conserved as well as the GGYC sequence. The numbering of the cysteine residues according to the defensin A and MGD-1 sequences is indicated above and below the sequences, respectively. X is for a modified amino acid. * indicates the hydroxylated tryptophan. (B) The lower sequence alignment between defensin A and MGD-1 highlights the hypothetical presence of the CS$\alpha\beta$ motif in MGD-1. Such a structural motif, which is the main structural feature of defensin A, is typically stabilized by three disulfide bonds. To match the C4−C25 disulfide bond of MGD-1 with the C3−C30 disulfide bond of defensin A, a deletion of seven residues was incorporated. The fourth disulfide bond between C21 and C38 which is characteristic of MGD-1 is displayed as a dotted line. Notice that a 36% level of sequence identity still remains for such an alignment.

showed that MGD-1 and MGD-2 contain in position 39 a glycine residue and that the C-terminus of at least MGD-1 was amidated. Nevertheless, despite the difference in the number of disulfide bonds, these four mollusk defensins display a high degree of sequence similarity (Figure 1). Moreover, they all contain in position 28 a modified residue, being identified as a hydroxylated tryptophan for MGD-1, which seems to be characteristic of mollusks.

On the basis of an alignment with the closest protein sequences, Hubert et al. (*12*) reported that MDG-1 bears the arthropod defensin signature. Indeed, MGD-1 and defensin A, a peptide of 40 amino acids with three disulfide bonds, isolated from *Phormia terranovae* larvae exhibit a level of sequence identity of 38.5%. The three-dimensional structure of defensin A was determined by NMR (PDB entry 1ica) and mainly consists of the CS$\alpha\beta$ motif (cystine-stabilized $\alpha-\beta$ motif), typically stabilized by three disulfide bonds (*8*, *14*).

The three-dimensional structure of the Mediterranean mussel defensin MGD-1 characterized by its four disulfide bonds has not yet been reported. From the sequence comparison with the insect defensin A, a hypothetical structure of MGD-1 was inferred. Given that it was very difficult to extract enough material to experimentally establish the three-dimensional structure of the native peptide, MGD-1 was synthesized. In this paper, we describe (i) the synthesis of MGD-1, (ii) its antibacterial activity, and (iii) its three-dimensional solution structure as determined by ^{1}H NMR. The CS$\alpha\beta$ motif of MGD-1 was compared with that of several proteins with various functions. Finally, the solution structure of MGD-1 was compared with that of defensin A and its antibacterial activity discussed in terms of the location of hydrophobic and positively charged residues (*15*).

MATERIALS AND METHODS

Isolation of the Native MGD-1. Native MGD-1 was isolated from *M. galloprovincialis* hemocyte granules as previously described (*13*).

Synthesis and Oxidation of MGD-1. Trifluoroacetic acid and acetonitrile (HPLC grade) were purchased from SDS (Peypin, France). All compounds used for solid-phase peptide synthesis (solvents, resins, and protected amino acids) were from Perseptive (Framingham, MA). MGD-1 peptide was synthesized in solid phase using the Fmoc strategy. The synthesis was carried out on a 0.2 mmol scale using a continuous flow apparatus (Perseptive, model 9050 PepSynthesizer) starting from Fmoc-PAL-PEG-PS resins as previously described (*16*) except that the coupling reaction was performed with 0.5 M TBTU in the presence of 1 M DIEA. After completion of the synthesis, side chain deprotections and the peptide cleavage were performed overnight with the K reagent (82.5% trifluoroacetic acid, 5% phenol, 5% thioanisole, and 2.5% ethanedithiol) at room temperature, and the crude peptide was purified by RP-HPLC.

The disulfide bridge formation was initially carried out at room temperature and monitored by analytical HPLC. By using the method described by Tam's group (*17*), oxidized MGD-1 containing the native arrangement of the four disulfide bonds was obtained in a rather low yield (≈3.5%) and purified by RP-HPLC. Treatment of the purified oxidized peptide with the Ellman reagent (*18*) showed the absence of free thiol groups. Then, air oxidation was carried out at a low temperature (4 °C), pH 6.2, and a concentration of 2 mg/mL in water. The progress of the oxidation reaction was monitored by ^{1}H NMR. Although the oxidation was much slower, the desired oxidized isomer was obtained with a 40% yield after 10 days. Oxidized MGD-1 was purified from the mixture by RP-HPLC.

The reduced and oxidized synthetic peptides were analyzed by both matrix-assisted laser desorption/ionization time-of-flight (MALDI-TOF) and electrospray ionization mass spectroscopy on a Bruker Biflex III and a Fisons TRIO 2000 (Birmingham, U.K.) mass spectrometer, respectively. For MALDI-TOF spectra, the α-cyano-4-hydroxycinnamic acid matrix was used. The spectrometers were calibrated using external standard peptides. Amino acid analyses and electrospray ionization mass spectra were in complete agreement with the proposed structure.

Antibacterial Assays. Antibacterial activity was monitored by a liquid growth inhibition assay (*19*). Briefly, 10 μL aliquots of native or synthetic defensin were incubated in microtiter plates with 100 μL of bacteria suspension (starting OD_{600} of 0.001) in Poor-Broth nutrient medium containing 1% bactotrypton and 5 g/L NaCl (pH 7.5). Bacterial growth was assayed by measurement of OD_{600} after incubation for 24 h at 30 °C. The minimal inhibitory concentration (MIC) was obtained by testing serial doubling dilutions of the peptides.

The minimal bactericidal concentration (MBC) was determined according to the method of Hancock (*20*). Peptides

were dissolved in a solution containing 0.01% acetic acid and 0.2% bovine serum albumin (BSA), and then serial doubling dilutions were made in this same solution. Aliquots (10 μL) from each dilution were incubated in sterile 96-well polypropylene microtiter plates with 100 μL of a suspension of bacteria (starting OD_{600} of 0.001) in Mueller Hinton Broth (MHB, Difco). Bacterial growth was checked after incubation for 18 h at 37 °C under agitation, except for the *Vibrio* species which were incubated at 25 °C in MHB supplemented with NaCl (15 g/L). The MBC was determined by plating the contents of the first three wells showing no turbidity onto MHB agar plates and incubating the plates at 37 °C for 18 h. The lowest concentration of peptide that prevented any residual colony formation corresponded to the MBC.

For kinetic assays, synthetic oxidized MGD-1 at 4 μM (10 times higher than the MIC) was added to an exponential growth-phase culture of *Micrococcus luteus*. Aliquots (100 μL) were removed at various times and plated on MHB agar plates, and the number of colony-forming units (cfu) was determined after incubation overnight at 37 °C.

Circular Dichroism. CD spectra of the reduced and oxidized forms of the synthetic MGD-1 were recorded at room temperature on a CD6 Jobin-Yvon spectrophotometer. Spectra were measured at pH 3.3 using a 1 mm path length cell on 200 μL of 3×10^{-5} and 12×10^{-5} M solutions of the oxidized and reduced forms of MGD-1, respectively. Each spectrum resulted from averaging five successive individual scans over the range of 195−250 nm.

NMR. ^2H_2O (99.95%) was purchased from the CEA (Saclay, France). The pH values were measured at room temperature with a 3 mm electrode and are uncorrected for the deuterium isotopic effect. The pH was adjusted by addition of 0.1 N HCl or 0.1 N NaOH. TSP-d_4 was added as an internal chemical shift reference at 0 ppm.

Native MGD-1 (0.2 mg) was dissolved in 0.4 mL of water (95/5 $H_2O/^2H_2O$), giving a 0.1 mM solution whose pH was adjusted to 3.0.

Lyophilized synthetic MGD-1 (2 mg) was dissolved in 0.15 mL of water (95/5 $H_2O/^2H_2O$) in a Shigemi tube. The pH of this 3 mM solution of MGD-1 was adjusted to 3.3.

Proton NMR experiments were performed on a Bruker AMX600 spectrometer, operating at 600 MHz, and recorded using a triple-resonance probe. In all experiments, the carrier frequency was set at the center of the spectrum at the water frequency. Most of the spectra were recorded at 285 K. DQF-COSY (*21*), z-TOCSY (*22*), and NOESY (*23*) spectra were acquired in the phase-sensitive mode using the States−TPPI method (*24*). For spectra recorded in H_2O, and except for the DQF-COSY spectra (where low-power irradiation was used), the water resonance was suppressed by the WATERGATE method (*25*). z-TOCSY spectra were obtained with a mixing time of 90 ms and NOESY spectra with mixing times of 100, 150, and 200 ms. The assignment of ambiguous connectivities was carried out with sets of spectra recorded at several temperatures ranging from 280 to 320 K.

In a second sample, MGD-1 was dissolved in 99.99% D_2O to identify slowly exchanging amide protons. The rate of exchange of amide protons was determined by following the disappearance of their signals from TOCSY and NOESY spectra recorded from 2 h to 4 days after dissolution.

Data were processed by using either UXNMR or GIFA (*26*) software. The data were zero-filled before processing, and shifted sine-bell functions were used for apodization. The processed data were baseline corrected using a five-order polynomial function. The identification of all the spin systems of MGD-1 was carried out by analysis and comparison of COSY, TOCSY, and NOESY spectra, and the full sequential assignment was achieved using the general strategy described by Wüthrich (*27*).

Structure Calculation. The NOESY cross-peaks were measured from the NOESY spectrum recorded with a mixing time of 100 ms and were divided into five classes, according to their intensities. Very strong, strong, medium, weak, and very weak NOEs were then converted into 1.8−2.4, 1.8−2.8, 1.8−3.6, 1.8−4.4, and 1.8−5.0 Å distance constraints, respectively. For equivalent protons or non-stereospecifically assigned protons, pseudoatoms were introduced. The Φ angle restraints were derived from the $^3J_{HN-C\alpha H}$ coupling constants, and the χ_1 and χ_2 angle restraints were derived from the combined analysis of the $^3J_{H\alpha-H\beta}$ and $^3J_{H\beta-H\gamma}$ coupling constants and intraresidue NOEs, respectively.

To determine three-dimensional structures, these distance and dihedral angle restraints were used as input in the standard distance geometry (DG)/simulated annealing (SA) refinement and energy-minimization protocol using the X-PLOR 3.1 program (*28*). In the first stage of the calculation, an initial ensemble of 50 structures was generated from a template structure with randomized backbone dihedral angles Φ and Ψ and extended side chains, using a DG protocol followed by restrained SA and refinement (*29*). Since the disulfide bond arrangement had to be determined, structures were generated without using any disulfide bond constraints. Analyzing the obtained structures and comparing them with the NMR data allowed us to identify more NOE restraints which were introduced into the subsequent calculation. After a number of these processes, 382 NOE-derived distance restraints (50 medium-range and 67 long-range) and 47 dihedral angles (19 Φ, 25 χ_1, and 3 χ_2) were used as the final input data. Analysis of the average $S\gamma-S\gamma$ distances in the lowest-energy structures allowed us to unambiguously determine the arrangement of the four disulfide bonds. Finally, a calculation including the disulfide bonds was carried out, and the resulting 21 structures with a minimum of restrained violations were submitted to 5000 cycles of restrained Powell energy minimization. The rms deviation calculations and visual display were performed with INSIGHT 97 (Molecular Simulation Inc., San Diego, CA). Hydrogen bonds were considered present if the distance between heavy atoms was less than 3.5 Å and the donor−hydrogen−acceptor angle was greater than 120°. The limits of the secondary structure elements and the van der Waals surfaces were determined with the STRIDE program (*30*). The coordinates of the refined conformers of MGD-1 are deposited in the PDB (entry 1FJN).

The lengths of the various elements of the CS$\alpha\beta$ motif of MGD-1 were compared with those of the structures sharing the similar fold available at the web site dedicated to the structural classification of proteins (http://scop.mrc-lmb.cam.ac.uk/scop/index.html) (*31*). The PDB entries of the 32 selected structures, which belong to the superfamily of scorpion-like toxins, include long-chain (2sn3, 1vna, 1nra, 1aho, 1cn2, 1bcg, 1snb, and 1b7d) and short-chain scorpion

toxins (1big, 1bkt, 2bmt, 1mtx, 1sxm, 2crd, 1scy, 1agt, 1tsk, 1pnh, 1acw, 1sco, 2ktx, 1lqi, 1bmr, 1lir, 1lqq, and 2pta), insect defensins (1myn and 1ica), plant defensins (1gpt, 1gps, and 1ayj), and brazzein (2brz).

RESULTS

Sequence Alignment and Structural Hypothesis. The MGD-1 sequence is characterized by its high cysteine (20.5%), glycine (20.5%), and arginine (12.8%) content. Together, these three amino acids represent 53.8% of the sequence. Among the remaining residues, the sequence contains nine hydrophobic residues (23.1%), including two prolines at positions 5 and 18. Moreover, mass spectroscopy showed that the tryptophan residue in position 28 is hydroxylated at C2 of the indole ring (*13*). MGD-1 displays a strong level of sequence similarity (up to 67.5%) with several defensin family peptides isolated from arthropods (*12*). Therefore, its disulfide bond pattern was inferred as being C4−C25, C10−C33, C14−C35, and C21−C38.

On the basis of the alignment with insect defensin A displayed in Figure 1A, MGD-1 presents a level of sequence identity of 38.5%, mainly including five of the eight cysteine residues, five of the eight glycine residues, and two of the five arginine residues. It is interesting to notice that the G^{22}-GYC^{25} tetrapeptide of MGD-1 is conserved in the four mussel defensins as well as in defensin A. Moreover, the spacing between four cysteine residues (C10, C14, C33, and C35) out of the five aligned cysteines strongly suggests that the MGD-1 structure contains the cystine-stabilized α-helical motif (CSH motif) observed in many peptides (apamin, endothelin, and scorpion toxins) and in defensin A (*32*). Indeed, the CSH motif consists of the typical CxxxC and CxC patterns located in helical and β-strand structures, respectively. Interestingly, the $C^{10}HRHC^{14}$ and the $C^{33}TC^{35}$ sequences of MGD-1 have been predicted to have an α-helical and a β-strand structure, respectively (*33*). Consequently, the alignment presented in Figure 1A strongly suggests the presence of the CSH motif in MGD-1 involving the C10−C33 and C14−C35 disulfide bonds.

However, when both the three-dimensional structure of defensin A and its disulfide pattern are taken into account, another alignment can be considered. This alignment is based on the hypothesis that the CSαβ motif, which is the main structural feature of the insect defensin A and which is typically stabilized by a third disulfide bond, is also present in MGD-1. On the basis of the initial alignment, C25 was supposed to belong to this additional disulfide bond with C4. Therefore, this third disulfide bridge (C4−C25) of MGD-1 would be equivalent to the C3−C30 disulfide bond of defensin A (Figure 1B). Notice that in both sequences this third disulfide bridge involves the N-terminal part. To perform such an alignment, in which C4 of MGD-1 matches with C3 of defensin A, a deletion of seven residues between C4 and C10 of MGD-1 sequence has to be invoked. It is interesting to notice that, for such a modified alignment, a 36% level of sequence identity still remains between MGD-1 and defensin A. Finally, on the basis of the location of cysteines and on the basis of their spacing in the sequence, it clearly appeared that the common CSαβ motif, which consists of one helical part and a β-sheet tightly linked together by the typical pattern of three disulfide bonds

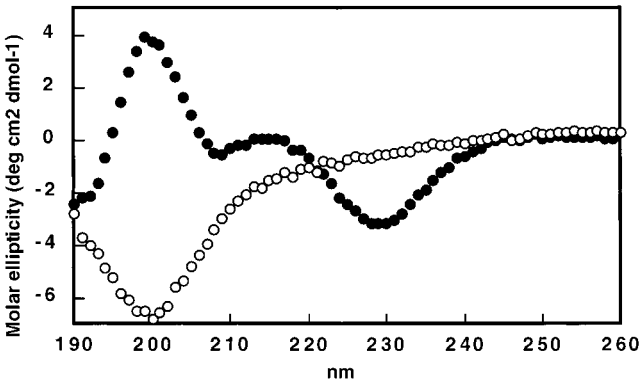

FIGURE 2: CD spectra of the reduced (○) and oxidized (●) forms of the synthetic MGD-1.

observed in defensin A, in numerous scorpion toxins, in one antifungal protein (*34*), and more recently in an antimicrobial protein (*35*), has to be present in the MGD-1 structure. On the basis of this new sequence alignment with defensin A, the three disulfide bridges (C4−C25, C10−C33, and C14−C35) are assumed to be involved in a CSαβ motif. Consequently, C21 and C38 must be involved in the fourth disulfide bond of the MGD-1 structure.

Synthesis and Disulfide Bond Formation in MGD-1. The reduced MGD-1 peptide was obtained in good yield by solid-phase synthesis using the Fmoc strategy. Then, the oxidized MGD-1 was analyzed by mass spectrometry, circular dichroism, and ^{1}H NMR spectroscopy. The molecular masses measured for the reduced (4409 Da, expected mass of 4407.15 Da) and oxidized (4397 Da, expected mass of 4399 Da) MGD-1 were in agreement with the formation of the four disulfide bridges.

The CD spectra of the reduced and oxidized forms of MGD-1 are displayed in Figure 2. The spectrum of the reduced form with a minimum at 200 nm is typical of an unstructured peptide, in agreement with the corresponding ^{1}H NMR spectrum (see below). On the contrary, the spectrum of the oxidized form is quite different and atypical with two minima at 229 (main) and 209 nm and two maxima at 199 (main) and 215 nm. Clearly, this spectrum results from a mixture of helical (typical minima at 208 and 222 nm and maximum at 193 nm) and β-sheet structures (typical maximum at 191−197 nm and minimum at 207−213 nm). Nevertheless, the minimum at 229 nm is unexpected due to the moderate contribution of helical and β-sheet structures at this wavelength. An attempt to calculate the percentage of secondary structures led to around 7% helix, 50% β-sheet, and 43% β-turn and random coil.

The ^{1}H NMR spectrum of the reduced MGD-1 displayed a weak dispersion of amide and methyl signals, which is typical of a nonstructured peptide (Figure 3B). On the contrary, the spectrum of its oxidized form exhibited a large spreading of the amide signals together with a dispersion of methyl signals, both indicating that this peptide was highly structured (Figure 3A). The correct arrangement of the four disulfide bonds was suggested by the similarity of its ^{1}H NMR spectrum and that of native MGD-1 isolated from hemocyte granules of *M. gallopro*v*incialis* as shown in Figure 3. Nevertheless, for the native MGD-1, in agreement with the hydroxylation of the W28 ring, the chemical shift of the indole proton signal (10.19 ppm) was significantly

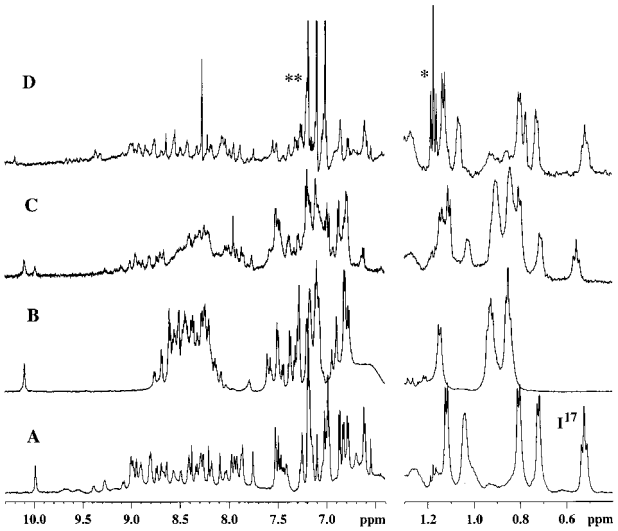

FIGURE 3: Low-field and high-field parts of one-dimensional ^{1}H NMR spectra of MGD-1 recorded at 300 K. (A) Spectrum of the synthetic oxidized MGD-1. (B) Spectrum of the synthetic reduced MGD-1. (C) Spectrum of the crude air oxidation milieu of synthetic MGD-1 after 10 days at 4 °C (2 mg/mL, pH 6.2). (D) Spectrum of the native MGD-1 purified from *M. galloprovincialis* hemocyte granules. Notice that the indole signal of the W28 displays different chemical shifts in the reduced and oxidized synthetic MGD-1. The δ CH_3 signal of I17 and the indole signal were used to monitor the progress of the formation of the native disulfide bonds. This is clearly observed in the 60/40 reduced/oxidized mixture of spectrum C. The indole signal of the native MGD-1 displays a slightly different chemical shift due to the C2 hydroxylation of the tryptophan ring (spectrum D) (*, impurity; **, signal for ammonium salt).

different from that measured for the synthetic peptide (9.98 ppm), MGD-1. Taking advantage of the fact that the ^{1}H NMR spectra of the reduced and oxidized forms of MGD-1 are quite different, we used NMR to monitor the progress of the oxidation step (Figure 3C). In this case, after 10 days, on the basis of the intensity of the indole signal, a yield of 40% was obtained (see the Discussion).

Antibacterial Activity. Native MGD-1 was reported as displaying antibacterial activity against both Gram-positive and Gram-negative bacteria (*12*). Antibacterial activities of native and synthetic MGD-1 (Table 1) were first measured against three Gram-positive and two Gram-negative bacteria and were found to be almost identical. Then, the antibacterial activity of the synthetic MGD-1 was measured on a larger number of bacteria strains. It clearly appeared that a similar activity was observed against all six Gram-positive bacteria that were tested, including human pathogens. In contrast, a very low antibacterial effect was observed against several Gram-negative bacteria, including *Vibrio* species which are pathogens for marine invertebrates. Therefore, we conclude that MGD-1 mainly displays a Gram-positive antibacterial effect. Moreover, the kinetics of the bacteriolytic activity were assayed on the Gram-positive *Mi. luteus* bacteria and showed that 99% of the bacteria were killed within <3 min of contact, proof of the important antibiotic capacities of such a peptide.

Structural Study of the Synthetic MGD-1. On the basis of the quite different spreading of amide and methyl signals, the ^{1}H NMR spectra of the reduced and oxidized MGD-1 (Figure 3) clearly indicated that the reduced peptide is nonstructured, whereas the oxidized one is highly constrained. Nevertheless, the C4−C25, C10−C33, C14−C35, and C21−C38 disulfide pattern of native MGD-1 inferred from the sequence similarity with peptides isolated from arthropods (*12*) and more precisely from the structure of defensin A (*14*) remained to be confirmed with experimental data. For this purpose, a structural study was carried out via ^{1}H NMR spectroscopy.

Table 1: Antibacterial Activities[a] of Native and Synthetic MGD-1

bacteria	activity	native MGD-1	synthetic MGD-1
Gram-positive			
Mi. luteus	MIC	0.6	0.4
	MBC	1.2	1.5
Bacillus megaterium	MIC	−	0.8
	MBC	−	1.5
Staphylococcus aureus	MIC	0.6	0.6
	MBC	1.2	1.2
Staphylococcus epidermidis	MIC	−	3.1
	MBC	−	6.2
Enterococcus fecalis	MIC	0.6	0.6
	MBC	1.2	1.2
Aerococcus viridans	MIC	−	0.4
	MBC	−	1.5
Gram-negative			
Escherichia coli D31	MIC	1.2	1.2
	MBC	1.2	1.2
E. coli 363	MIC	0.6	1.2
	MBC	1.2	1.2
Salmonella newport	MIC	−	>100
	MBC	−	>100
Vibrio alginolyticus	MIC	−	50
	MBC	−	>100
Vibrio harveyi	MIC	−	50
	MBC	−	100
Vibrio metshnikovii	MIC	−	>100
	MBC	−	>100

[a] The activities are expressed in terms of micromoles per liter.

NMR Study. Classical two-dimensional spectra (TOCSY, COSY, and NOESY) of synthetic MGD-1 were recorded at several temperatures ranging from 280 to 320 K to facilitate the full assignment that was carried out according to the strategy described by Wüthrich (*27*). The ^{1}H spectrum of MGD-1 is characterized by a large spread of the amide and α-protons, leading to a strong dispersion of cross-peaks in the fingerprint area of the COSY and TOCSY experiments. However, despite this cross-peak spreading, difficulties were encountered for the assignment in three parts of the sequence. The first difficulty encountered arose from the numerous Gly and Cys residues in the sequence (41% of the sequence) and from the presence of the two CGG tripeptides in positions 22−24 and 25−27, respectively ($C^{21}GGYCGG^{27}$ segment) (Figure 1). Two other ambiguities arose from the full assignment of residues P5 and R30. They were clarified upon analysis of two-dimensional spectra recorded at 280, 290, 300, and 320 K. Two parts of the NOESY spectra are displayed in Figure 4, and the summary of NOEs is displayed in Figure 5.

To locate the elements of secondary structure, chemical shifts of the α-protons were compared with statistical chemical shifts determined for a random coil conformation (*36*−*39*). The chemical shift deviations are reported in Figure 5. Positive deviations were measured for the R20−G26 and R32−C38 segments, suggesting that they adopt a β-strand structure. On the contrary, negative deviations suggesting an helical structure were measured for the N7−S16 sequence.

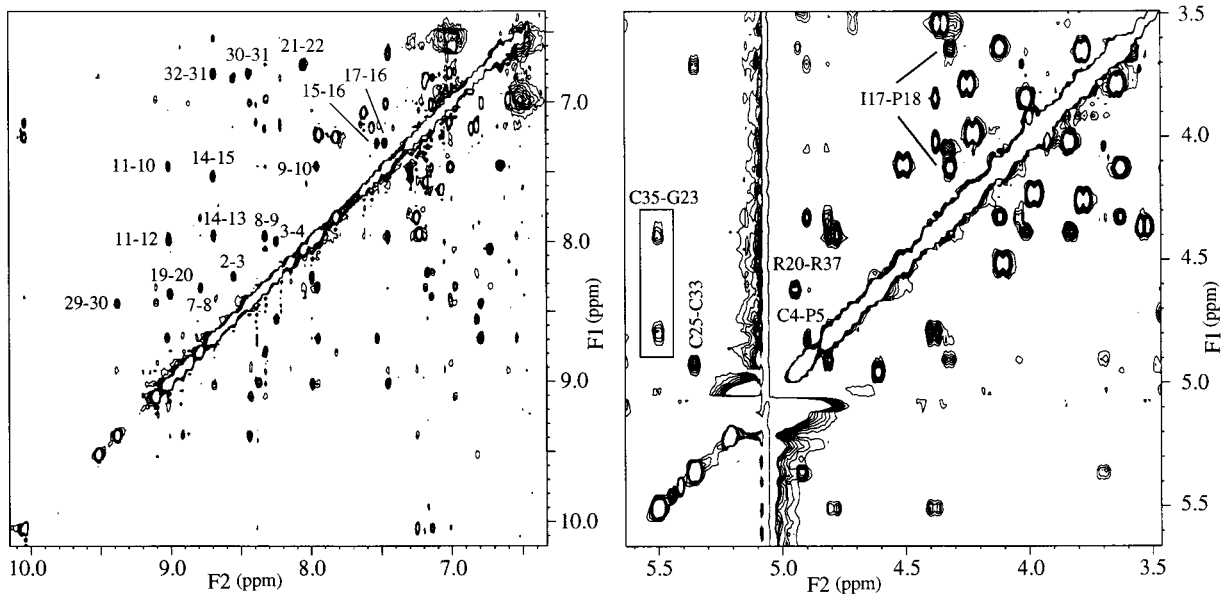

FIGURE 4: NOESY spectra of synthetic MGD-1. (Left) Part showing the amide−amide NOEs mainly due to the helical structure (pH 3.3, 285 K, mixing time of 200 ms). (Right) Part of the spectrum recorded in deuterated water showing α−α NOEs typical of the *β*-sheet (277 K, mixing time of 100 ms). The NOEs that allowed the determination of the cis conformation of the C4−P5 amide bond (dαα C4−P5) and the trans conformation of the I17−P18 amide bond (dα*δ* I17−P18) are also labeled.

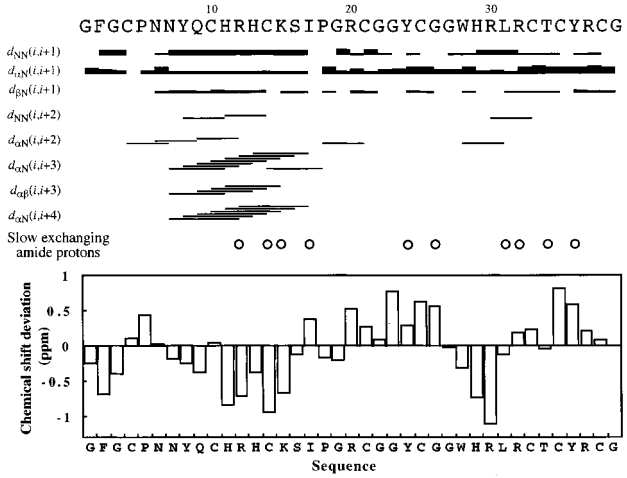

FIGURE 5: Summary of NOE data, slow exchanging amide protons, and chemical shift deviations of the α-protons measured for synthetic MGD-1. In the upper part, the thickness of the bars indicates the intensity of the NOEs; the slow exchanging amide protons are denoted with empty circles. In the lower part, negative and positive deviations are indicative of helical and *β*-strand structures, respectively.

The short W28−L31 sequence also displayed a negative deviation, indicative of either a short helix or a turn.

When the compound was solubilized in deuterated water, the signals of 10 amide protons (R12, C14, K15, I17, Y24, G26, L31, R32, T34, and Y36) were still observed after 20 h, strongly suggesting that they are involved in significant hydrogen bonds. The summary of these slow exchanging amide protons is displayed in Figure 5.

Determination of Structures. MGD-1 structures were determined by using the XPLOR program, and 382 NOE-derived distances and 47 dihedral constraints were used as input. Since the disulfide pattern of MGD-1 remained to be determined, disulfide bond constraints were not taken into account in preliminary calculations. On the basis of the distance between *β*-carbons of the eight cysteine residues, the disulfide linkages were unambiguously established as being C4−C25, C10−C33, C14−C35, and C21−C38. A final run of calculation was carried out, including this disulfide pattern arrangement, and the 21 lowest-energy conformers of the 50 calculated were retained and analyzed. Limits of secondary structure elements were determined by using the STRIDE program. This family of structures is shown in Figure 6, and the structure statistics are summarized in Table 2. These structures are well-defined all along the sequence, and the pairwise mean rms deviations for the backbone and heavy atoms were 0.34 ± 0.08 and 1.14 ± 0.13 Å, respectively. The distribution in the Ramachandran plot of all residues of the 21 best structures indicates their quality: 89.7% in the most favored regions and 10.3% in the additional allowed regions (*40*). The global structure of MGD-1 has an approximately cylindrical shape with a 13−18 Å diameter and a 28−32 Å height. The obtained structures consist of an α-helical part (residues 7−16) and a slightly twisted *β*-sheet made up of two antiparallel strands. Strand I (residues 20−25) is roughly antiparallel to the helix, and strand II (residues 33−37) is roughly parallel to the helix (Figures 6 and 7). The sequence linking the α-helix and strand I (17−19/20 residues) includes a distorted type II turn, whereas the loop connecting the two *β*-strands (residues 26−32) includes a type III′ turn. The helix and *β*-sheet axes differ by an angle of 40−50°. The helix and strand II are cross-linked by the C10−C33 and C14−C35 disulfide bridges localized in the core of the molecule, giving rise to a typical CSH motif. Moreover, the structure is strongly constrained by the two other disulfide bridges located in two opposite parts of the molecule. The C4−C25 disulfide bridge connects the N-terminal segment with the last residue of strand I, whereas the C21−C38 disulfide bridge, specific for MGD-1, connects the N- and C-terminal parts of the two *β*-strands. The arrangement of the three disulfide bonds (C4−C25, C10−C33, and C14−C35) is typically that of the CSα*β* motif. Moreover, the distribution of the four disulfide bridges connecting the two elements of secondary structure (helix

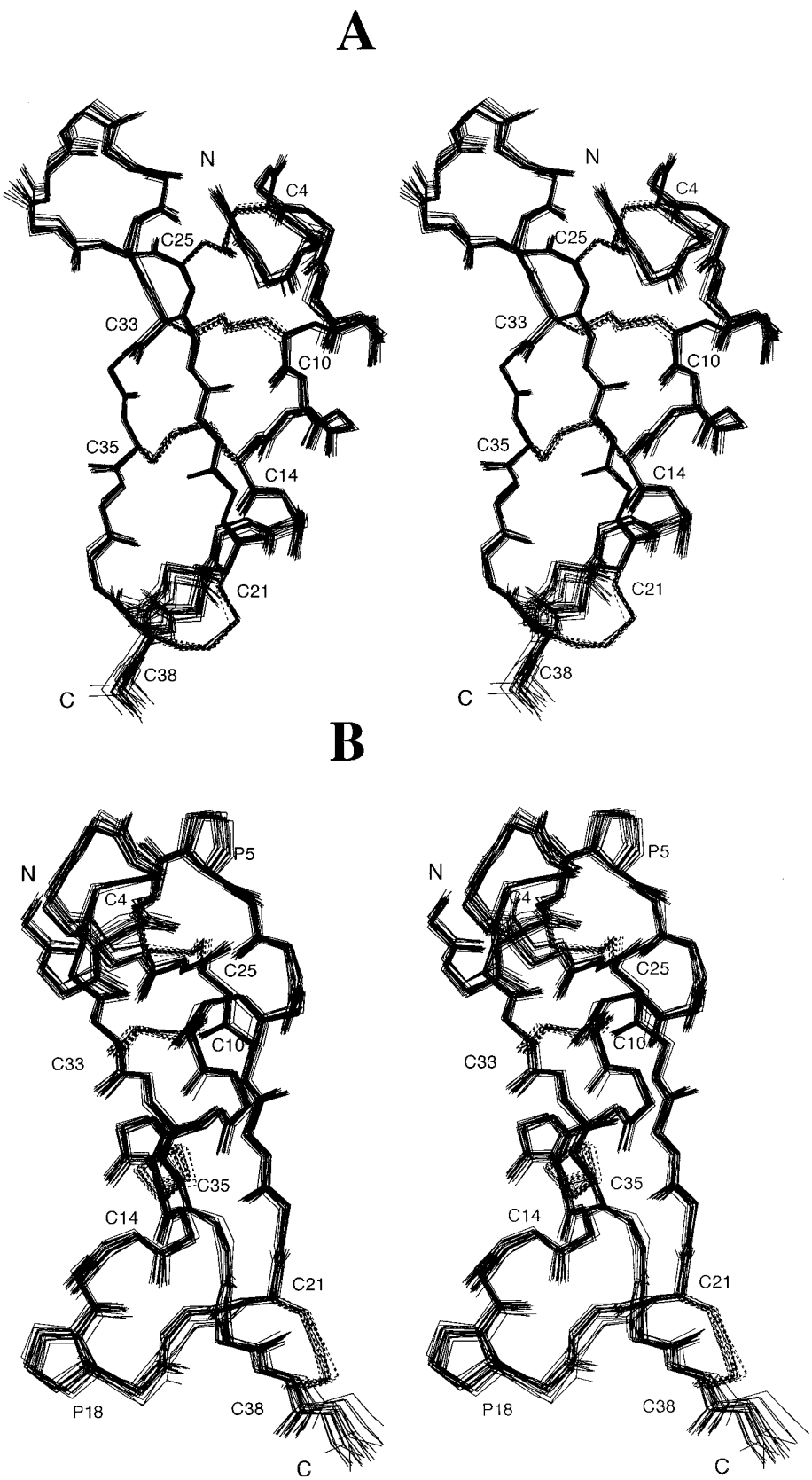

FIGURE 6: Two stereoviews 90° apart of the 21 best energy-minimized conformers representing the solution structure of MGD-1. The heavy atoms of the backbone were used for the superimposition. The four disulfide bridges are labeled and displayed as dashed lines. (A) Backbone and disulfide bonds. (B) This stereoview shows the location of the two proline residues at the top (P5, cis amide bond) and at the bottom (P18, trans amide bond). The average angle between the helix and the β-sheet is about 50°.

and β-sheet) lead to a highly constrained structure. This is confirmed by the very low level of exchange measured for 10 amide protons involved in hydrogen bonds. Four hydrogen bonds between R12, C14, K15, and I17 amide protons and Y8, C10, H11, and H13 carbonyl groups, respectively, are located in the helical part, and four hydrogen bonds involving

Table 2: Experimental and Structural Statistics for the Family of 21 Structures of MGD-1[a]

no. of distance restraints	
intraresidue ($i - j = 0$)	122
sequential ($i - j = 1$)	143
medium-range ($i - j \leq 5$)	50
long-range ($i - j > 5$)	67
total	382
no. of dihedral angle restraints	
ϕ	19
χ_1	25
χ_2	3
total	47
mean rms deviations from experimental restraints	
NOE (Å)	0.0338 ± 0.0021
dihedrals (deg)	0.413 ± 0.137
mean rms deviations from idealized covalent geometry	
bonds (Å)	0.004 ± 0.001
angles (deg)	0.627 ± 0.003
impropers (deg)	0.296 ± 0.009
mean energies (kJ/mol)	
E_{NOE}	6.58 ± 0.83
E_{cdih}	0.13 ± 0.08
E_{vdW}	-59.32 ± 3.46
E_{bond}	9.17 ± 0.26
$E_{improper}$	4.64 ± 0.31
E_{angle}	62.64 ± 0.56
E_{elec}	-138.45 ± 3.54
E_{total}	-114.85 ± 4.88
pairwise atomic rms differences (Å)	
backbone atoms (1−39)	0.34 ± 0.08
heavy atoms (1−39)	1.14 ± 0.13

[a] For these calculations, the XPLOR all-hydrogen force fields topoallhdg and parallhdg all were used. The final minimization of the 21 structures was carried out with force constants of 15 kcal mol^{-1} Å^{-2} and 50 kcal mol^{-1} rad^{-2} for the NOE and dihedral angle potentials, respectively.

Y24, G26, T34, and Y36 amide protons and T34, R32, Y24, and G22 carbonyl groups, respectively, are located in the β-sheet structure. The L31 and R32 amide protons both hydrogen bond with the W28 carbonyl group in the loop joining the two β-strands.

DISCUSSION

Improvement of the Yield of the Oxidation Step. Most of time, linear peptides with lengths of ≤40−50 amino acids can be obtained by solid-phase synthesis. However, for peptides containing disulfide bonds, the oxidation step leading to the expected disulfide bond pattern is not very well controlled. Therefore, the low yield of the oxidation step becomes the bottleneck of the synthesis and if unsuccessful can abolish the successful synthesis of the reduced peptide. Although the conformations of intermediates can markedly differ, in several cases it has been shown that the disulfide bonds buried in the folded conformation are formed in the slowest step, whereas those at the surface of the molecule are formed in the most rapid step (*41*, *42*). With regard to defensin peptides containing the CS$\alpha\beta$ motif, only the synthesis of the *Chironomus* defensin A (three disulfide bonds, sequence 55% similar with that of the *Phormia terranovae* larvae defensin A) has been reported to date (*43*). The authors reported that the one-step formation of all disulfide bridges mainly resulted in oligomerization. Finally, they used a tedious two-step strategy to form the three disulfide bonds in a controlled fashion. After they formed the C3−C26 disulfide bond, the formation of the two other disulfide bonds was facilitated (33% yield). With this strategy, they obtained the oxidized defensin with a 7% yield for total synthesis. It should be noted that defensin A, whose structure has been established by NMR, was overexpressed in *Saccharomyces cerevisae* probably to overcome the folding step (*14*).

It is usually considered that the formation of disulfide bonds occurs in a thermodynamically controlled process (*44*), and rarely is the isomer of interest obtained alone. With regard to MGD-1 and when the various combinations of the four-disulfide pairing are taken into account, 105 isomers were potentially expected. At room temperature, whatever the oxidative reagent, we systematically obtained an insoluble compound, probably a polymer due to the high reactivity of several thiolate anions (*42*). Indeed, it has been reported that the presence of positively charged residues near the cysteine residues decreases their pK_a value and therefore increases their reactivity. This is clearly the case for four (C^{14}K, RC^{21}, RC^{33}, and RC^{38}) of the eight cysteine residues of MGD-1. Finally, although in a low yield (≈3.5% after purification by HPLC), the oxidized MGD-1 was obtained by using DMSO as the oxidative reagent as described by Tam et al. (*17*). This low yield contrasts with the high efficiency of the folding of proteins which bear the CS$\alpha\beta$ motif, like in charybdotoxin (*45*).

Assuming that the native disulfide isomer is the most stable and that disulfide bonds are formed in a thermodynamically controlled step, we carried out the oxidation at a low temperature (4 °C) in a slightly acidic medium (pH 6.2), first to slow the kinetics, therefore facilitating the shuffling of the disulfide bonds, and second to favor formation of the native isomer. Moreover, under these conditions, the formation of intermolecular disulfide bonds was expected to be minimized. The disulfide bond formation was monitored by ^{1}H NMR by observation of the methyl signals as well as that of the indole proton, both of which have typical chemical shifts in the reduced and the oxidized forms of MGD-1. Surprisingly, these conditions were found to yield the desired isomer in a quite interesting yield (40%) when compared with the very low yield initially obtained at room temperature and at higher pH values (Figure 3C). This large improvement in the yield of the formation of native disulfide bond confirms that in this case the native isomer is significantly more stable than the others. A similar dramatic effect of the temperature was observed in the oxidative folding of the ω-conotoxin MVIIC (*46*).

The folding of MGD-1 can be compared with that of the Cn5 scorpion toxin which gives a very low yield in vitro of the native fold under the usual conditions, implying that in vivo the folding is assisted by chaperones and specific enzymes. Although its structure has not yet been determined, on the basis of its sequence similarity with the Cn2 toxin (PDB entry 1cn2) (*47*), its structure probably consists mainly of the CS$\alpha\beta$ motif fold. Moreover, the Cn2 structure contains a cis amide bond (W58−P59) in a sequence conserved in Cn5, suggesting that a cis amide bond is also conserved in Cn5. Fersht's group clearly demonstrated that folding of the Cn5 in the presence of a minichaperone (fragment of GroEL), proline isomerase (PPI), or disulfide isomerase (DsbA) was not greatly improved by any one of these proteins alone. In contrast, the folding becomes much more efficient (≤87%) in the presence of all three proteins, suggesting that they

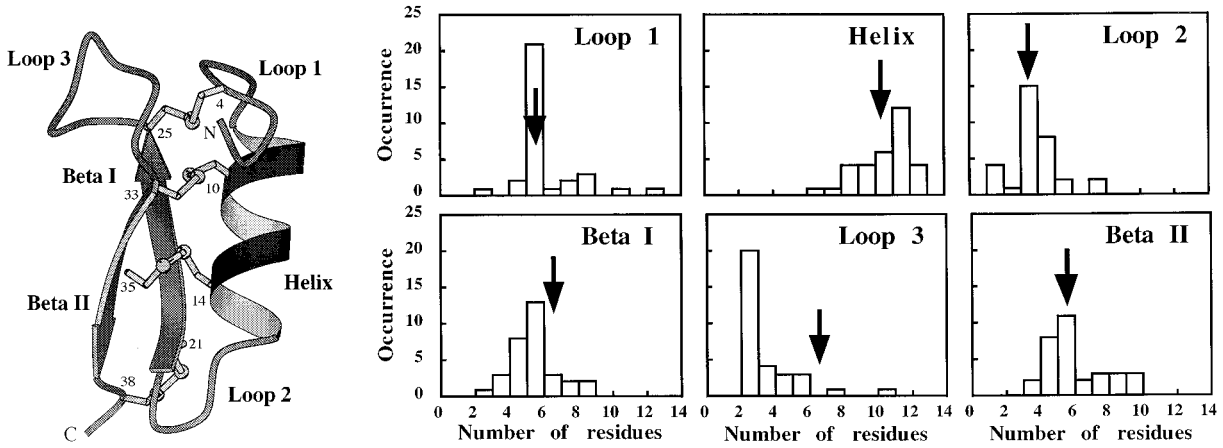

FIGURE 7: Comparison of the lengths of the various elements of secondary structures of MGD-1 with those statistically observed in 32 structures containing the CSαβ motif. Their locations are indicated on the structure prepared using MOLSCRIPT (*53*). Their lengths were determined with the STRIDE program. Loop 1 was defined as the section joining the cysteine residue equivalent to the Cys4 of MGD-1 to the beginning of the helix. The vertical black arrows indicate the lengths of the various elements of secondary structures measured for MGD-1.

exert a cooperative effect by acting simultaneously on the limiting steps of the folding of Cn5 scorpion toxin (*48*). In the case of MGD-1, both a slightly acidic medium, which decreases the difference in reactivity of the thiolate anions, and a low temperature significantly slow the kinetics of folding. Although the oxidation step takes several days under these conditions, this approach is much easier to perform when compared with the tedious double protecting group strategy used for the synthesis of the *Chironomus* defensin A (*43*) or by using the minichaperone, PPI, and DsbA mixture (*48*).

The activities of both the synthetic and native MGD-1 are similarly oriented principally toward Gram-positive bacteria. Moreover, this similarity of antibacterial potency indicates that hydroxylation of the tryptophan in position 28 is not important for the antibacterial activity. Finally, the similarity of the ^{1}H NMR spectra and the similarity of the antibacterial activity suggest that synthetic and native MGD-1 have the same three-dimensional structure.

Solution Structure of MGD-1. The MGD-1 structure as determined by ^{1}H NMR mainly consists of the CSαβ motif as deduced from the sequence alignment with the defensin A sequence. The CSαβ motif is made up of an α-helical part (residues 7−16) and of a slightly twisted β-sheet made up of two strands (Figure 6). Strand I (residues 20−25) is roughly antiparallel to the helix, and strand II (residues 33−37) is roughly parallel to the helix. Loop 2 (17−19/20 residues) includes a distorted type II β-turn [$\Phi(i+1) = -76°$, $\Psi(i+1) = 137°$, $\Phi(i+2) = 82°$, and $\Psi(i+2) = 37°$], whereas loop 3 (residues 28−31) includes a type III′ β-turn [$\Phi(i+1) = 57°$, $\Psi(i+1) = 32°$, $\Phi(i+2) = 58°$, and $\Psi(i+2) = 28°$] (*49*). The various elements of secondary structure are tightly cross-linked together by the four disulfide bonds regularly divided up from the top to the bottom of the molecule (Figure 6).

MGD-1 contains eight aromatic residues, three tyrosines (Y8, Y24, and Y36), three histidines (H11, H13, and H29), one phenylalanine (F2), and one tryptophan (W28). Interestingly, the ring of the three histidine residues is close to another aromatic ring. Clearly, the H13 ring stacks with the F2 ring (Cγ−Cγ distance = 4.1 Å) and the H19 ring with the W28 ring (Cγ−Cγ distance = 4.4 Å). Although only separated by one helix turn, a larger distance is measured between the H11 and the Y8 rings (Cγ−Cγ distance = 6.9 Å).

Conformation of the Four Disulfide Bridges of MGD-1. It is noteworthy that the three disulfide bridges of the CSαβ motif are located in the core of the molecule and contribute to its hydrophobicity. Indeed, the exposed areas of the C4−C25, C10−C33, and C16−C35 disulfide bridges are only 33.4, 11.8, and 13.6 Å^2, respectively. In contrast, the fourth disulfide bond (C21−C38), typical of the MGD-1 structure, is exposed to the solvent by an area of 118.1 Å^2. With regard to their geometry, C4−C25, C14−C35, and C21−C38 disulfide bridges have χ_3 angle values of −85.2°, −61.5°, and −58.1°, respectively. These values are those of the classical conformation of disulfide bridges (±90 ± 45°) (*50*). In contrast, the C10−C33 disulfide bond displays an average unusual χ_3 angle value of −161.4°. It is interesting to note that in CSαβ-related structures (see below), χ_3 angle values of ±180 ± 30° were measured for the equivalent disulfide bridge for four structures (1lqq, 2pta, 1myn, and 2crd) out of the 32 structures that were selected. Moreover, a similar observation was reported for the equivalent disulfide bridge (C22−C47) in 60% of the brazzein structures (2brz) (*51*). Taken together, these observations suggest that the disulfide bridge in this position can frequently adopt a noncanonical conformation.

Conformation of the Two Prolines. MGD-1 contains two prolines, a residue known to be unfavorable in both helical and β-strand structures and therefore mainly located in loops and turns. In agreement with this general observation, P5 and P18 are located in loops upstream and downstream from the helix, respectively (Figure 6B). The analysis of constraints clearly revealed that the I17−P18 amide bond adopts a trans conformation, whereas the C4−P5 amide bond adopts a cis conformation. The conformation of the latter is characterized by the HαC4−HαC5 NOE typically observed for such a conformation (Figure 4). It is interesting to notice that the probability of X being a cysteine in the cis X−Pro amide bond is low; in this position, a proline or an aromatic residue is most frequently observed (*52*). Therefore, it can be assumed that in this case, the cis conformation of the amide bond better satisfies constraints in this part of the

molecule due mainly to the C4−C25 disulfide bond.

CSαβ Motif of MGD-1. The lengths of the helix, the two β-strands, and various loops of the Csαβ motif of MGD-1 were compared with those of molecules containing the same motif. For this purpose, 32 structures were selected from the structural classification of protein folds in the superfamily of scorpion-like toxins. This selection includes long-chain and short-chain scorpion toxins and insect and plant defensins. The length of the various structural elements (helix, loop, and β-strand) was determined using the STRIDE program. The results of this analysis are displayed in Figure 7 and compared with the results for MGD-1. It appears that the length of five of these structural elements (loop 1, the helix, loop 2, β-strand I, and β-strand II) corresponds to the most frequently encountered length of these elements, indicating that the CSαβ motif of MGD-1 is similar to the average length for a CSαβ motif. In contrast, loop 3 (six residues) is much longer than the two residues, the most frequently observed in the selected structures (Figure 7). Despite this latter difference, the MGD-1 structure has to be classified in the superfamily of scorpion-like toxins. Nevertheless, its specificity lies in the presence of the unusual fourth disulfide bond (C21−C38) which joins the beginning of β-strand I and the end of β-strand II and is solvent-exposed (see above). In contrast, the three other disulfide bonds are located in the hydrophobic core of the molecule. Therefore, with its four disulfide bonds and the hydrogen bond network, the MGD structure is highly constrained.

A similar structure, consisting of the CSαβ fold, stabilized by four disulfide bonds, was reported for the potassium channel blocking toxin (38 residues) from the *Pandinus imperator* scorpion (PDB entry 1qky) (*54*) and recently for another short scorpion toxin, HsTX1 (34 residues), acting also as a potassium channel inhibitor (this structure is not yet available; PDB entry 1quz) (*55*). In contrast, for the maurotoxin, which belongs to the same toxin family, surprisingly a quite different disulfide pattern was reported (*56*). Although the MGD-1 and 1qky sequences are quite different, they contain six positively charged and four aromatic residues, and their structures share a similar global shape. Nevertheless, they significantly differ in the location of the positively charged residues at their surface. This large difference in the distribution of positively charged, negatively charged (absent in MGD-1), and hydrophobic residues is probably responsible for their difference in activity, one displaying antibacterial activity (MGD-1) and the other acting on potassium channels.

As described above, a disulfide bond equivalent to the fourth C21−C38 disulfide bond of MGD-1 is rarely observed in proteins bearing the CSαβ fold. Nevertheless, although it is shortened in its N-terminal part, it is interesting to compare the MGD-1 structure with those of the antifungal proteins (1ayj and 1myn) and the plant defensin (1gps), which share a similar global fold and display four disulfide bonds, three of them being located in the CSαβ motif. Surprisingly, the fourth disulfide bond, which is located in the same region in all these structures, is topologically different in MGD-1 (C21−C38) than in the other proteins (C4−C51 for 1ayj, C2−C44 for 1myn, and C3−C47 for 1gps). Indeed, in all these structures, one cysteine residue located in the C-terminal part of the strand II is conserved, whereas the other cysteine is located either on strand I (C21 for MGD-1) or on the extended N-terminal sequence (C4 for 1ayj, C2 for 1myn, and C3 for 1gps). This structural observation suggests a common ancestral molecule which evolved differently. The shortening of the N-terminal sequence could lead to either the disappearance of this disulfide bond (many toxins display only the three disulfide bonds of the CSαβ motif) or the formation of a new one by mutation to cysteine of a residue in the close environment of the conserved cysteine of the C-terminal part of β-strand II. This could be the case for C21 in MGD-1 located in β-strand I. The observation of a similar disulfide pattern both in mollusks and in some scorpions is in agreement with such a common ancestral molecule. Moreover, a phylogenetic analysis of defensins is indicative of a slow evolutionary process in mussels, scorpions, and dragonflies, but a fast evolutionary process for neopteran insects (*11*).

Comparison of MGD-1 and Defensin A Structures. On the basis of the comparison of different peptides, Kini and Evans (*15*) put forward the hypothesis that the spatial proximity of a cationic site to a hydrophobic site should be a structural requirement for cytolytic activity. Indeed, a cationic cluster flanked by hydrophobic cluster appears to be a common structural feature shared by numerous cytolytic peptides such as sapecin, magainin, human defensin, and cardiotoxins (*15* and references therein). Known to be very important in antibacterial peptides, the distribution of the hydrophobic and charged residues was considered in the defensin A and MGD-1 structures since both molecules display an antibacterial activity.

First of all, we have shown that the structure of MGD-1 contains the CSαβ structural motif hypothesized from the alignment of MGD-1 and defensin A sequences (Figure 1B). From the comparison of these two antibacterial molecules which share the common Csαβ motif, it appears that the MGD-1 structure is more compact than that of defensin A, for which a hinge motion has been reported for N-terminal large loop 1 (*14*). The MGD-1 and defensin A structures mainly differ by the presence of a fourth disulfide bond, possibly rendering MGD-1 more stable in high-osmolarity medium (seawater) with a shorter loop 1, resulting from a deletion of seven residues, and by the high content of aromatic residues [eight for MGD-1 instead of three for defensin A (Figures 1 and 8)]. These differences increase the compactness of the MGD-1 structure, even if the two structures have very similar surfaces, 3091 Å^2 for MGD-1 and 3098 Å^2 for defensin A.

Defensin A and MGD-1 possess four basic residues (R23, R26, K33, and R39) and six basic residues (R12, K15, R20, R37, R30, and R32), accounting for 699 and 905 Å^2 of the surface, respectively (Figures 1 and 8). Interestingly, the location of two of the four basic side chains in the left part of the defensin A structure is conserved in the MGD-1 structure. On the top of the molecule, K33 can be considered equivalent to R30 in MGD-1. At the bottom of the structure, the R23 side chain in front of the molecule is located in a position similar to that of the R20 and R37 side chains in MGD-1. In contrast, neither the R26 nor the R39 side chain of defensin A is located in the same region as the R32 side chain of MGD-1. The MGD-1 structure contains two additional positively charged residues which are located on the right side of the molecule in the helical part (R12 and K15).

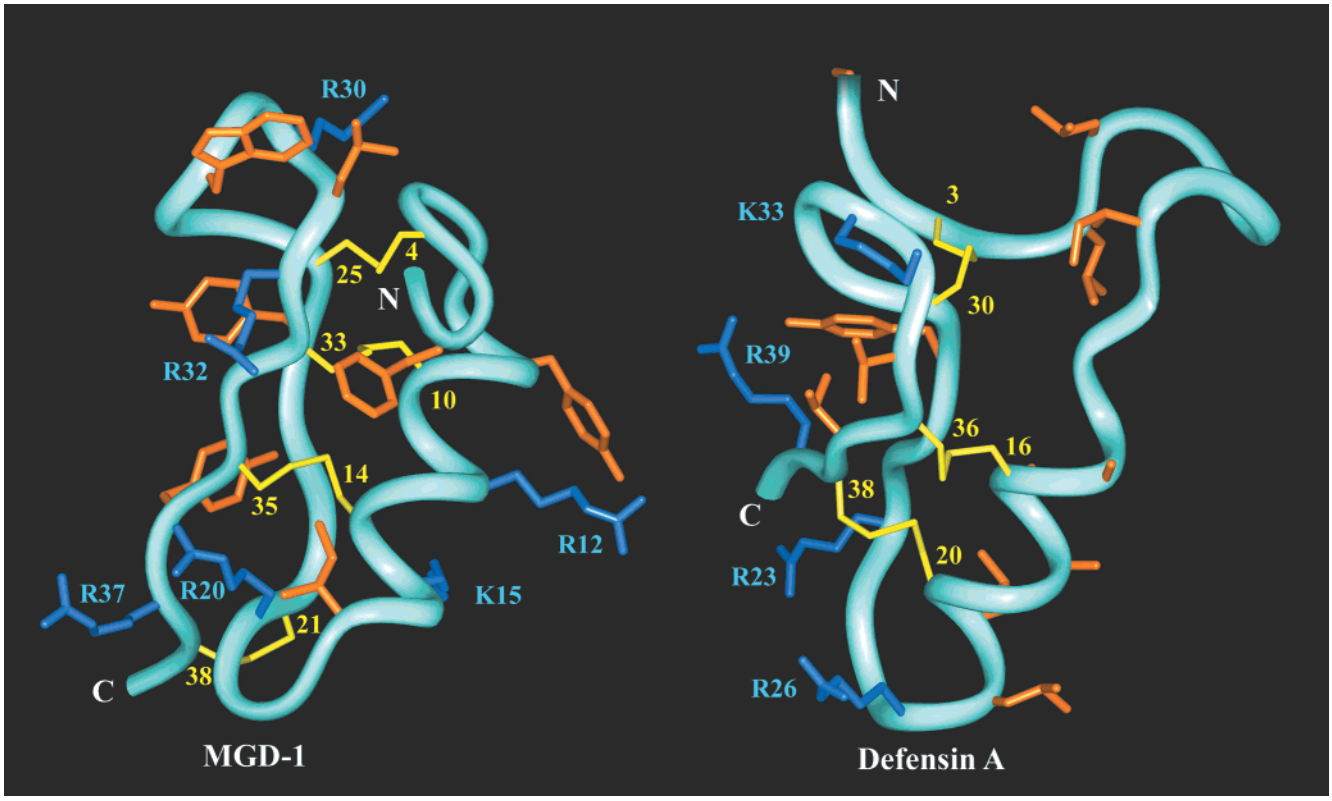

FIGURE 8: MGD-1 and defensin A (PDB entry 1ica) solution structures showing the location of the hydrophobic (orange) and positively charged (blue) side chains. Disulfide bonds are represented with dashed lines. For the sake of clarity, only Arg and Lys side chains are labeled. In the MGD-1 structure, the hydrophobic ring of P5 and P18 is not displayed (see Figure 6B).

With regard to the hydrophobic residues, it clearly appears that the helix of defensin A is particularly hydrophobic compared with the MGD-1 helix. Both structures have a hydrophobic core mainly due to the disulfide bonds (see above). Defensin A displays a large hydrophobic cluster including the helix (from the bottom to the top, L22, L21, A17, and A15) extended to the large N-terminal loop (I11, L5, and L6) (Figure 8). Despite the two basic residues in the helix (R12 and K15), the MGD-1 structure also displays a large hydrophobic area, including the P18, I17, F2, W28, L31, P5, and Y8 residues on the front of the molecule, whereas Y24 and Y36 are located to the rear of the molecule (Figure 8). Interestingly, the size of the hydrophobic surface in the two molecules is very similar (1106 Å^2 for MGD-1 and 1124 Å^2 for defensin A). Moreover, it is interesting to note that the Y24 residue of MGD-1 and the Y29 residue of defensin A belong to the conserved tetrapeptide GGYC and, moreover, that the two tyrosine side chains are similarly oriented in the two structures. Although the role of the glycine residues is not clearly defined in antibacterial peptides, it is worth noting that the positions of G27, G28, G24, and G32 of defensin A are conserved in the MGD-1 structure (G22, G23, G19, and G27, respectively).

There is no doubt that MGD-1 and defensin A share some common properties in the distribution of hydrophobic and hydrophilic side chains which could explain their activity against Gram-positive bacteria. Their significant structural differences, particularly in the additional positively charged residues in the helical part and in the presence of the fourth disulfide bound in MGD-1, do not appear to affect this activity. Nevertheless, to gain further insights into the structure−activity relationship of MGD-1, we plan to study the antibacterial activity of the R12A/K15A analogue, in which the two positive charges will be removed, and of the C21S/C38S analogue, containing the three arthropod-equivalent disulfide bonds.

ACKNOWLEDGMENT

We thank Nathalie Galeotti for her help in recording MALDI-TOFF spectra and are indebted to Dr. S. L. Salhi for the editorial revision of the manuscript.

REFERENCES

1. Bulet, P., Hetru, C., Dimarcq, J. L., and Hoffmann, D. (1999) *Dev. Comp. Immunol. 23*, 329−344.
2. Epand, R. M., and Vogel, H. J. (1999) *Biochim. Biophys. Acta 1462*, 11−28.
3. Ganz, T., and Lehrer, R. I. (1994) *Curr. Opin. Immunol. 6*, 584−589.
4. Lehrer, R. I., and Ganz, T. (1999) *Curr. Opin. Immunol. 11*, 23−27.
5. Tang, Y. Q., Yuan, J., Osapay, G., Osapay, K., Tran, D., Miller, C. J., Ouellette, A. J., and Selsted, M. E. (1999) *Science 286*, 498−502.
6. Hetru, C., Hoffman, J. A., and Bulet, P. (1998) in *Molecular Mechanisms of Immune Response in Insects* (Brey, P. T., and Hultmark, D., Eds.) pp 40−66, Chapman & Hall, London.
7. Garcia-Olmedo, F., Molina, A., Alamillo, J. M., and Rodriguez-Palenzuela, P. (1998) *Biopolymers 47*, 479−491.
8. Bonmatin, J. M., Bonnat, J. L., Gallet, X., Vovelle, F., Ptak, M., Reichhart, J. M., Hoffmann, J. A., Keppi, E., Legrain, M., and Achstetter, T. (1992) *J. Biomol. NMR 2*, 235−256.
9. Zhang, X. L., Selsted, M. E., and Pardi, A. (1992) *Biochemistry 31*, 11348−11356.
10. Pardi, A., Zhang, X. L., Selsted, M. E., Skalicky, J. J., and Yip, P. F. (1992) *Biochemistry 31*, 11357−11364.

11. Charlet, M., Chernysh, S., Philippe, H., Hetru, C., Hoffmann, J. A., and Bulet, P. (1996) *J. Biol. Chem. 271*, 21808−21813.
12. Hubert, F., Noel, T., and Roch, P. (1996) *Eur. J. Biochem. 240*, 302−306.
13. Mitta, G., Vandenbulcke, F., Hubert, F., and Roch, P. (1999) *J. Cell Sci. 112*, 4233−4242.
14. Cornet, B., Bonmatin, J. M., Hetru, C., Hoffmann, J. A., Ptak, M., and Vovelle, F. (1995) *Structure 3*, 435−448.
15. Kini, M. R., and Evans, H. J. (1989) *Int. J. Pept. Protein Res. 34*, 277−286.
16. Aumelas, A., Mangoni, M., Roumestand, C., Chiche, L., Despaux, E., Grassy, G., Calas, B., and Chavanieu, A. (1996) *Eur. J. Biochem. 237*, 575−583.
17. Tam, J., Wu, C., Liu, W., and Zhang, J. (1991) *J. Am. Chem. Soc. 113*, 6657−6662.
18. Ellman, G. L. (1959) *Arch. Biochem. Biophys. 82*, 70.
19. Bulet, P., Cociancich, S., Dimarcq, J.-L., Lambert, J., Reichhart, J.-M., Hoffmann, D., Hétru, C., and Hoffmann, J. A. (1991) *J. Biol. Chem. 266*, 24520−24525.
20. Hancock, B. (1997) http://www.cmdr.ubc.ca/bobh/MIC.htm and http://www.interchg.ubc.ca/bobh/methods.htm.
21. Rance, M., Sorensen, O. W., Bodenhausen, G., Wagner, G., Ernst, R. R., and Wuthrich, K. (1983) *Biochem. Biophys. Res. Commun. 117*, 479−485.
22. Rance, M. (1987) *J. Magn. Reson. 74*, 557−564.
23. Macura, S., Huang, Y., Sutter, D., and Ernst, R. R. (1981) *J. Magn. Reson. 43*, 259−281.
24. Marion, D., Ikura, M., Tschudin, R., and Bax, A. (1989) *J. Magn. Reson. 85*, 393−399.
25. Piotto, M., Saudek, V., and Sklenar, V. (1992) *J. Biomol. NMR 2*, 661−665.
26. Pons, J. L., Malliavin, T. E., and Delsuc, M. A. (1996) *J. Biomol. NMR 8*, 445−452.
27. Wüthrich, K. (1986) in *NMR of Proteins & Nucleic Acids*, John Wiley & Sons, New York.
28. Brünger, A. T. (1992) *X-PLOR version 3.1: A system for X-ray crystallography and NMR*, Yale University Press, New Haven, CT.
29. Nilges, M., Clore, G. M., and Gronenborn, A. M. (1988) *FEBS Lett. 229*, 317−324.
30. Frishman, D., and Argos, P. (1995) *Proteins 23*, 566−579.
31. Murzin, A. G., Brenner, S. E., Hubbard, T., and Chothia, C. (1995) *J. Mol. Biol. 247*, 536−540.
32. Tamaoki, H., Miura, R., Kusunoki, M., Kyogoku, Y., Kobayashi, Y., and Moroder, L. (1998) *Protein Eng. 11*, 649−659.
33. Fischer, D., Barret, C., Bryson, K., Elofsson, A., Godzik, A., Jones, D., Karplus, K. J., Kelley, L. A., MacCallum, R. M., Pawowski, K., Rost, B., Rychlewski, L., and Sternberg, M. (1999) *Proteins Suppl. 3*, 209−217.
34. Fant, F., Vranken, W., Broekaert, W., and Borremans, F. (1998) *J. Mol. Biol. 279*, 257−270.
35. Fant, F., Vranken, W. F., and Borremans, F. A. (1999) *Proteins 37*, 388−403.
36. Wishart, D. S., Sykes, B. D., and Richards, F. M. (1991) *J. Mol. Biol. 222*, 311−333.
37. Lee, M. S., Palmer, A. G., III, and Wright, P. E. (1992) *J. Biomol. NMR 2*, 307−322.
38. Wishart, D. S., and Sykes, B. D. (1994) *Methods Enzymol. 239*, 363−392.
39. Wishart, D. S., Bigam, C. G., Holm, A., Hodges, R. S., and Sykes, B. D. (1995) *J. Biol. NMR 5*, 67−81.
40. Laskowski, R. A., MacArthur, M. W., Moss, D. S., and Thornton, J. M. (1993) *J. Appl. Crystallogr. 26*, 283−291.
41. Creighton, T. E. (1995) *Philos. Trans. R. Soc. London, Ser. B 348*, 5−10.
42. Creighton, T. E. (1997) *Biol. Chem. Hoppe-Seyler 378*, 731−744.
43. Lauth, X., Nesin, A., Briand, J. P., Roussel, J. P., and Hetru, C. (1998) *Insect Biochem. Mol. Biol. 28*, 1059−1066.
44. Gilbert, H. F. (1994) in *Mechanisms of Protein Folding* (Pain, R. H., Ed.) pp 104−136, IRL Press, Oxford, U.K.
45. Drakopoulou, E., Vizzavona, J., Neyton, J., Aniort, V., Bouet, F., Virelizier, H., Menez, A., and Vita, C. (1998) *Biochemistry 37*, 1292−1301.
46. Kubo, S., Chino, N., Kimura, T., and Sakakibara, S. (1996) *Biopolymers 38*, 733−744.
47. Pintar, A., Possani, L. D., and Delepierre, M. (1999) *J. Mol. Biol. 287*, 359−367.
48. Altamirano, M. M., Garcia, C., Possani, L. D., and Fersht, A. R. (1999) *Nat. Biotechnol. 17*, 187−191.
49. Smith, J. A., and Pease, L. G. (1980) *CRC Crit. Rev. Biochem.*, 315−399.
50. Srinivasan, N., Sowdhamini, R., Ramakrishnan, C., and Balaram, P. (1990) *Int. J. Pept. Protein Res. 36*, 147−155.
51. Caldwell, J. E., Abildgaard, F., Dzakula, Z., Ming, D., Hellekant, G., and Markley, J. L. (1998) *Nat. Struct. Biol. 5*, 427−431.
52. Pal, D., and Chakrabarti, P. (1999) *J. Mol. Biol. 294*, 271−288.
53. Kraulis, P. J. (1991) *J. Appl. Crystallogr. 24*, 946−950.
54. Delepierre, M., Prochnicka-Chalufour, A., Boisbouvier, J., and Possani, L. D. (1999) *Biochemistry 38*, 16756−16765.
55. Savarin, P., Romi-Lebrun, R., Zinn-Justin, S., Lebrun, B., Nakajima, T., Gilquin, B., and Menez, A. (1999) *Protein Sci. 8*, 2672−2685.
56. Blanc, E., Sabatier, J. M., Kharrat, R., Meunier, S., el Ayeb, M., Van Rietschoten, J., and Darbon, H. (1997) *Proteins: Struct., Funct., Genet. 29*, 321−333.

BI0011835